Chapter 8
Dynamic four-point bend fracture with a modified Split Hopkinson (Kolsky) Bar

Aishvarya Joshi, Cody Kirk, Tyler Dillard, Matthew Kappes, Zherui Martinez-Guo

Abstract High-rate deformation and fracture behavior of aerospace-grade alloys, such as Ti-6Al-4V and Al 2024, are important for understanding their performance under extreme loading conditions. The objective of our study is to design an experimental setup and investigate the dynamic fracture behavior of these alloys using a modified Split Hopkinson Pressure Bar (SHPB) setup integrated with a four-point bend fixture to evaluate Single Edge Notched Bend (SENB) specimens with different triaxiality are tested to analyze their respective fracture strain. The experiments are conducted for high-strain-rate conditions, with Digital Image Correlation (DIC) used to measure local strain fields and ABAQUS simulations to determine stress triaxiality. Pulse shaping techniques are implemented to ensure dynamic equilibrium and minimize inertial effects. The results would demonstrate a dependence of fracture behavior on notch geometry and strain rate, providing valuable data for developing high-fidelity material models that predict failure across various geometries.

Keywords SHPB · Triaxiality · Fracture · Bending · Material model

Introduction

Titanium and aluminium alloys are widely used in the aerospace industry due to their exceptional properties that meet the stringent requirements of aircraft and spacecraft. Among the most widely utilized alloys, Ti-6Al-4V and Al 2024 are particularly favoured for their high strength, durability, and resistance to extreme forces and structural damage with low weights, making them ideal for aerospace applications, especially for turbine blades which endure extreme environmental conditions under high speeds. Ti-6Al-4V is an α+β phase alloy, which is its most stable form of Ti-6Al-4V alloy, provides high strength when heat-treated [3]. Similarly, Al 2024-T351 is used for its high strength-to-weight ratio [4]. Despite Ti-6Al-4V and Al 2024's wide usage in the aerospace applications, there is a lack of understanding of the fracture and crack initiation for local features. The failure progression in Ti-6Al-4V and Al 2024 under high strain-rate loading begins with elastic deformation, where experimental force-displacement data and strain measurements show strong agreement with numerical simulations. As the load increases, the material transitions into plastic yielding, where localized plastic strain accumulation at the notch tip begins to develop. Following plastic deformation, crack initiation occurs at regions of maximum stress concentration, which shows variation in from standard behavior in simulations due to strain rate sensitivity and microstructural heterogeneity. This emphasizes the need for refined failure models to better capture the transition to fracture. Hence, it is important to evaluate the changes in their material properties and performance at such conditions.

Lesuer et al. evaluated the ability of the Johnson-Cook model to represent the deformation and failure response of these materials under conditions relevant to simulations of engine containment and the influence of uncontained engine debris on aircraft structures [5]. Despite challenges such as time-consuming calibration, failure criteria simulations are gaining traction in the aerospace, automotive, and manufacturing industries [3] [4]. These failure criteria enable impact damage simulation and residual integrity assessment, aiding in aerospace crashworthiness analysis.

Aishvarya Joshi(✉) · Cody Kirk · Tyler Dillard · Zherui Martinez-Guo
School of Aeronautics & Astronautics Engineering, Purdue University, West Lafayette, IN, USA
e-mail: joshi270@purdue.edu; kirk24@purdue.edu; tdillard@purdue.edu; zmg@purdue.edu

Zherui Martinez-Guo
School of Materials Science Engineering, Purdue University, West Lafayette, IN, USA
e-mail: zmg@purdue.edu

Matthew Kappes
Rolls-Royce Corporation, 450 South Meridian Street, Indianapolis, IN, USA
e-mail: Matthew.Kappes@Rolls-Royce.com

Paul Allison et al. (eds.), *Dynamic Behavior of Materials, Vol. 1*, Conference Proceedings of the Society for Experimental Mechanics Series, https://doi.org/10.13052/97887-438-0827-5_8

One of the failure criteria that researchers have explored is the Bao–Wierzbicki framework which further enhances the predictive capabilities of failure models, and it incorporates stress triaxiality as a key parameter. Fracture calibration of Ti-6Al-4V and Al 2024 using this framework to characterize ductile failure criteria represents a state-of-the-art approach based on stress triaxiality. Since stress triaxiality depends on the geometry of the specimen, this method provides an effective way to correlate geometry with material properties and predict failure [6]. The development and refinement of advanced material models for Al 2024 T3 and Ti-6Al-4V have also been done by DOT/FAA/TC-13/25 P1, P2, P3 [15][16][17] and DOT/FAA/TC-15/23 [18] respectively where material model parameters for input in LS-DYNA for simulation are in parallel with mechanical experiments under various strain rates. Damage due to tensile and compression, high energy - dynamic loading on both materials is analyzed and reported to create a material model for different loading conditions. Metal plasticity and fracture modeling methodology with the help of experimental data is also described in this research [19][20][21]y. Evaluations using hat-shaped specimens for the stress triaxiality and fracture strain have been conducted by Wang et al. [7]. However, crack initiation at high triaxialities under high strain rates in Single Edge Notched Bend (SENB) specimens is a field that provides an opportunity for further research.

Experimental techniques such as the Split Hopkinson Pressure Bar (SHPB) provide a controlled method for investigating these fracture phenomena under high strain rates. A Split Hopkinson Pressure Bar, also called as the Kolsky bar, is an experimental setup used to conduct experiments under high rate loading under laboratory-controlled conditions to obtain dynamic response of materials. In this setup, two elastic rods were placed on either side, with one struck by the striker under pressure from the gas gun. As shown in the schematic Figure 2, the rod between the striker and specimen is the incident bar, while the rod on the other side is the transmission bar. When the incident bar is struck, a compressive stress wave propagates toward the specimen, moving the bar material as it passes. Upon reaching the interface, part of the wave reflects into the incident bar, while the rest transmits through the specimen into the transmission bar. Laboratory instrumentation records these waves—both the incident wave and its reflection, as well as the wave in the transmission bar—allowing for a consistent and quantitative impact event. By varying the impact velocity and specimen size, different strain rates can be achieved. Further analysis of the recorded waves provides insights into loading conditions and specimen deformation states [2].

To dynamically load and evaluate the Single Edged Notch Bend Specimen or SEN(B) specimen under high strain rates, an SHPB setup was modified incorporating four-point bend fixtures as shown in Figure 2. This kind of setup has been illustrated in Weerasooriya et al. and Henschel et al. [1] [8]. This study focuses on evaluating Ti-6Al-4V and Al 2024 at high strain rates for different triaxiality values. Fracture strain is determined using Digital Image Correlation (DIC), while triaxiality factors are obtained through ABAQUS simulations. These results are correlated to develop a material model capable of predicting fracture behavior at high strain rates across various geometries.

Background

Specimen Configuration

The specimen geometry was designed in accordance with ASTM E399-23 (*Standard Test Method for Linear-Elastic Plane-Strain Fracture Toughness of Metallic Materials*) [9], specifically Annex A3.2, which outlines special requirements for testing Single Edge Notched Bend (SENB) specimens. The specimen dimensions were scaled down in accordance with the Kolsky bar dimensions available in our facility. Additionally, ASTM E23-34 (*Standard Test Methods for Notched Bar Impact Testing of Metallic Materials*) [10], which provides specifications for impact testing of U – notch specimens, was referenced for the design of U notches with the SEN(B) configuration with variation in triaxiality.

Table 1 presents the calculated parameters derived from these standards. Simulation results indicated no significant variation in the stress triaxiality factor for notches with equal radii, highlighting notch radius as the primary factor influencing triaxiality variation across specimens. Accordingly, five different notch radii, ranging from 0.15 mm to 1.5 mm, were selected for testing. Figure 1 illustrates the specimen dimensions.

The spacing of the support pins and load pins were according to ASTM C1161-18 [11]. The fixtures are made of A2 Steel heat treated according to ASTM A681-08 [12]y. The hardness of the fixtures measured after the heat treatment was 62 HRC. Hertzian Analysis was done to predict the elastic indentation stress limit for the hardened fixtures which was calculated to be 2.41GPa [13]. To minimize the wave disturbances caused by the introduction of the fixtures, the wave impedance of the fixtures should match with those of the bars, $(\rho cA)_{fixtures} = (\rho cA)_{bar}$ to minimize the wave disturbances caused by the introduction of the fixtures [2]. Since the density and wave speed in Kolsky bars and fixtures is the same, the cross-section area of the fixtures was matched to that of the Kolsky bars. The fixtures were attached to the Kolsky bar using support collars made of Aluminum 6061-T6.

Table 1 Dimensions calculation based on ASTM E399-23 standards

Parameter	**Value (mm)**	**Criterion**
Width W	9	Size of Kolsky Bar
Thickness B	4.5	B = $W/2$
Length L	37.8	L = 4.2W
Notch length a	4.1	$0.45 \leq a/W \leq 0.55$
Notch Radii R	0.15, 0.3, 0.65, 1, 1.5	Stress triaxiality variation

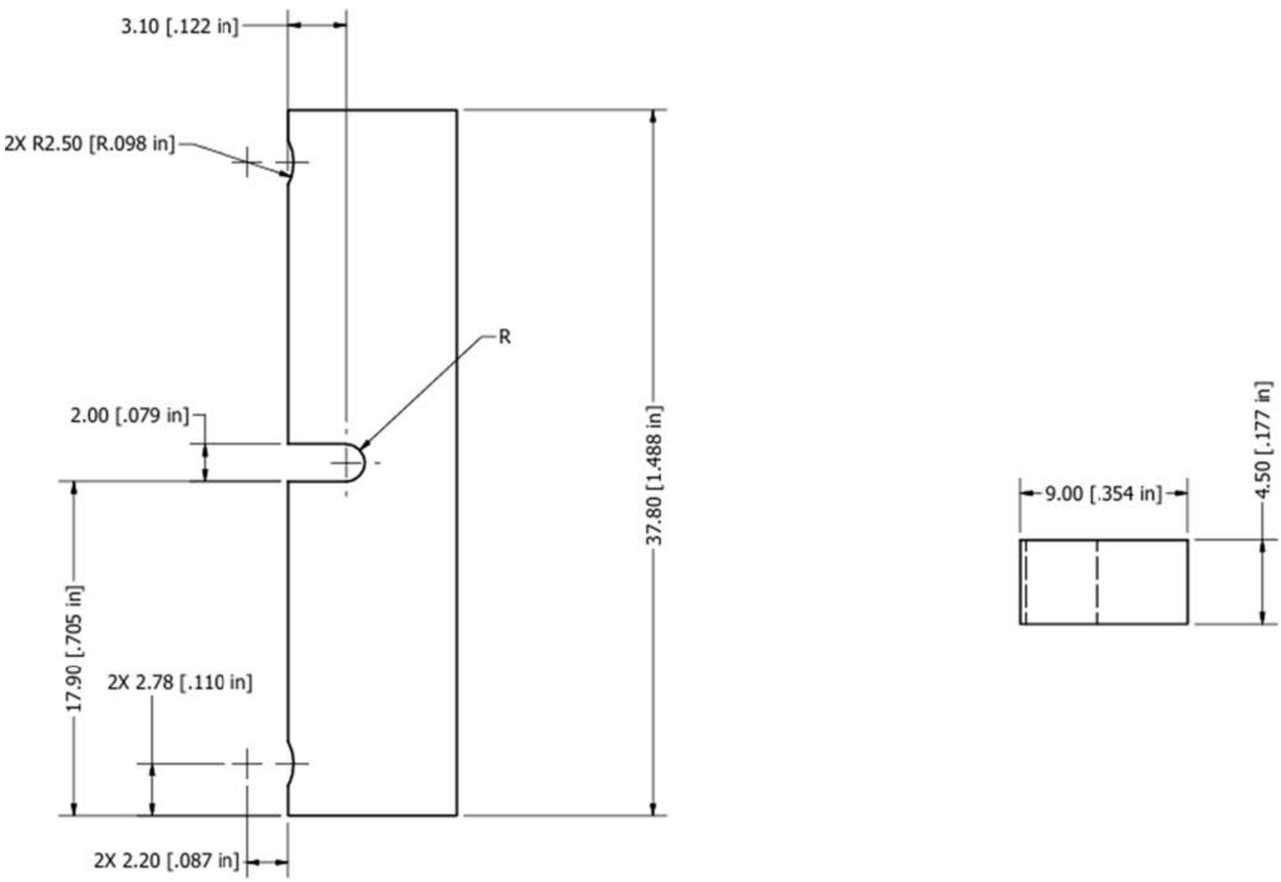

Fig. 1 Specimen Configuration with R varying as 0.15mm, 0.3mm, 0.65mm, 1mm and 1.5mm

High-Rate Testing Setup

The Kolsky Bar in our experimental setup is made of C300 Steel. The wave speed in the bar is calculated as $C_{bar} = \sqrt{\frac{E}{\rho}}$ where $E = E_{bar}$(Elastic modulus of C300 Steel) and $\rho = \rho_{bar}$(Density of C300 Steel). Ambient temperature is maintained for the experiments.

The specimen undergoing fracture needs to be in dynamic equilibrium and needs to fracture at a constant strain rate. It is crucial to initiate the crack in the specimen at the first pulse to get accurate measurements of local fracture strain at the constant strain rate applied. To have a gradual ramp in loading and give enough time for the specimen to come in equilibrium, a copper pulse shaper of thickness 4.7mm and the diameter $\frac{1}{4}$ inches was used. The velocity of incident bar was 9.83 m/s. Figure 4 shows the ramp loading and the duration of incident loading in two different pulse shapers where initially a thinner copper pulse shaper was used (thickness = 1.7mm). However, the loading duration was too short for that. Eventually, increasing the thickness of the pulse shaper to 4.7mm gave us the incident loading we wanted,

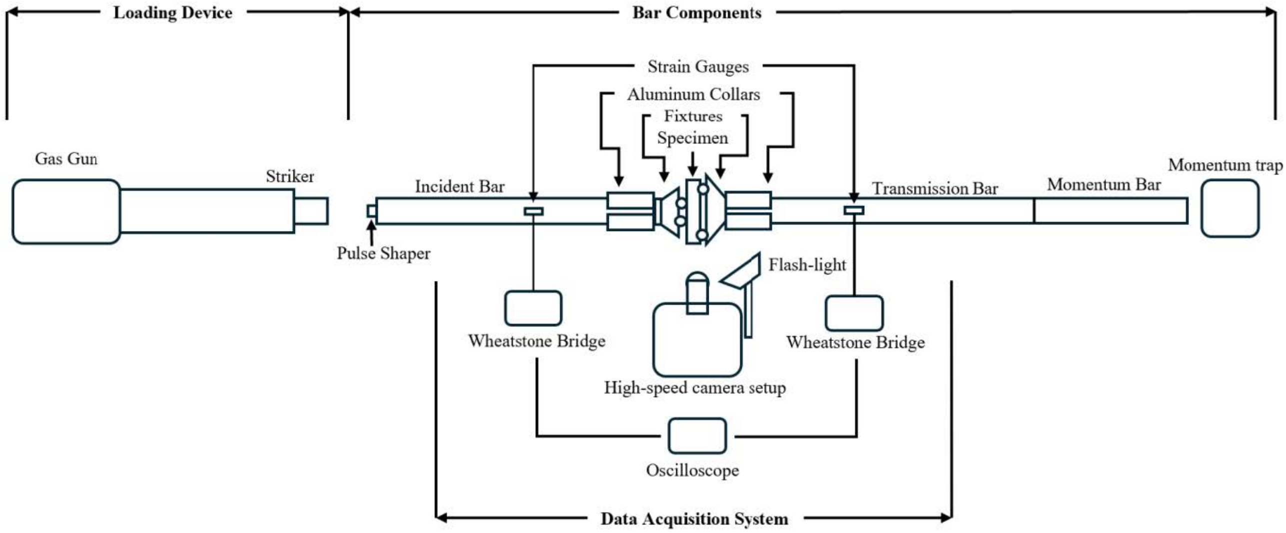

Fig. 2 Schematic of the experimental setup

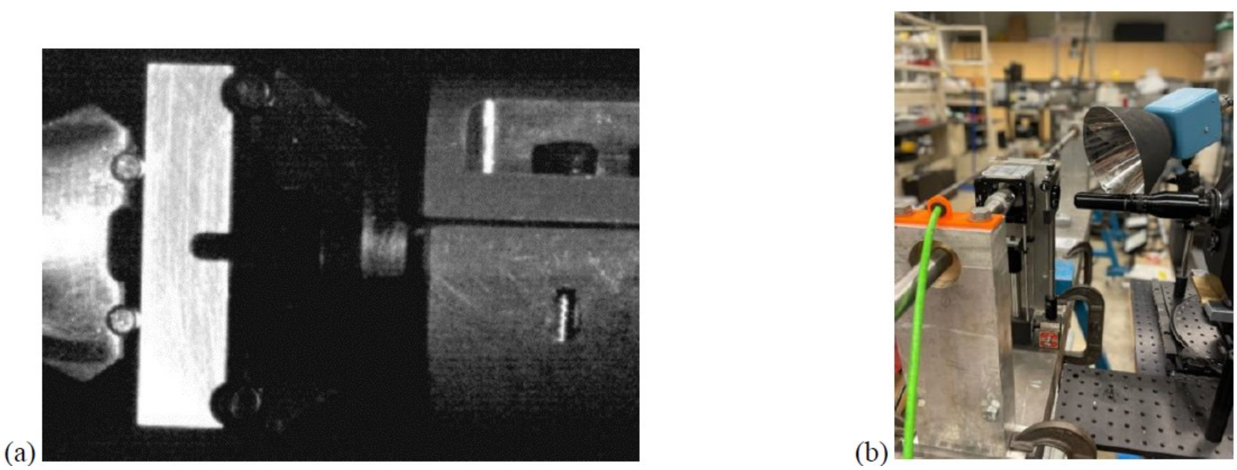

Fig. 3 (a) 4-point bend setup (b) Kolsky bar with Shimadzu Camera and Flash Lamp setup

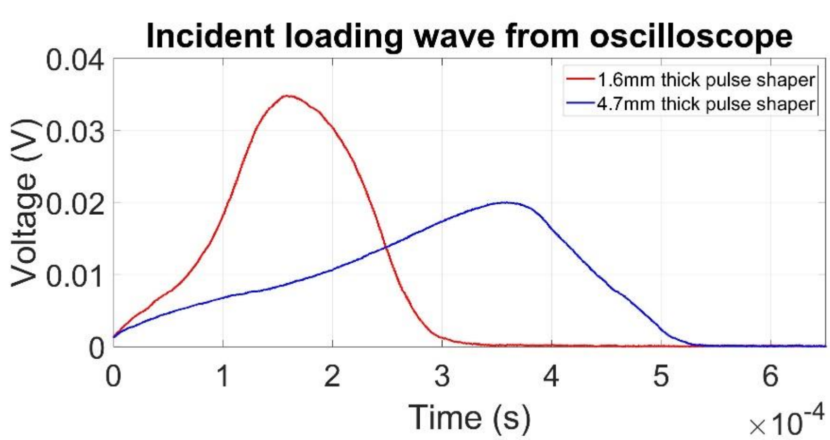

Fig. 4 Plot depicting increase in loading duration due to change in thickness of pulse shaper

Analysis

Resonant frequency analysis

To determine the upper limit in loading rate under which equilibrium is ensured, it is necessary to determine the first resonant frequency of the specimen within the specific boundaries of the experimental setup. If the highest frequency component of the loading pulse is much higher or lower than the first resonant frequency, the specimen is approximately in its equilibrium state. To estimate the first resonant frequency of the specimen in the modified SHPB setup, the experimental configuration is modeled as a multi-body dynamic system, with reference to Weerasooriya et al [1]. In this simplified model, the specimen is represented by a single-degree mass-spring system with mass m and elastic constants K1 and K2. A1 and A2 are cross sectional areas, E1 and E2 are Young's moduli, and $\rho 1$ and $\rho 2$ are material densities of the incident bar and the material respectively. The forces F1 and F2 are loads acting on both sides of the specimen. A dynamics analysis with details given in [1], reveals that the transfer function between F1and F2 has the following form in equation E1:

$$H(\omega_n) = \frac{F_2}{F_1} = \frac{1}{1 - \frac{m\omega_n^2}{K_1} + i\frac{m\omega_n^2}{K_2 E_2 A_2}} \quad \text{(E1)}$$

As shown in Figure 5 (a) and 5(b), the first resonant frequency is 93.2 kHz. The base frequency of the loading pulse is estimated by performing FFT (Fast Fourier Transform) on the loading signal and estimated it to be around 2000Hz as shown in Figure 6 (a) and 6(b), which is below the resonant frequency. The transfer function H thus has a value close to unity as can be observed in Figure 5 (a) and 5 (b) at all frequency values before the resonant frequency.

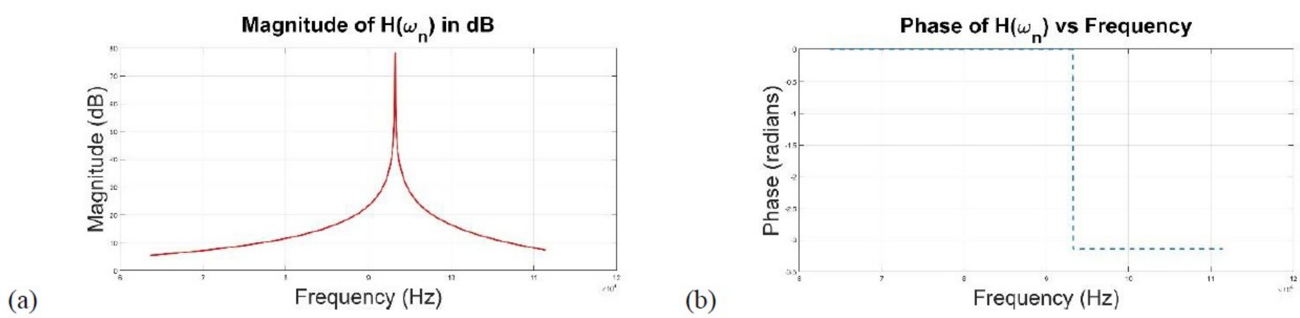

Fig. 5 (a) and (b) are plots of H vs Frequency depicting resonance frequency at 93.2kHz.

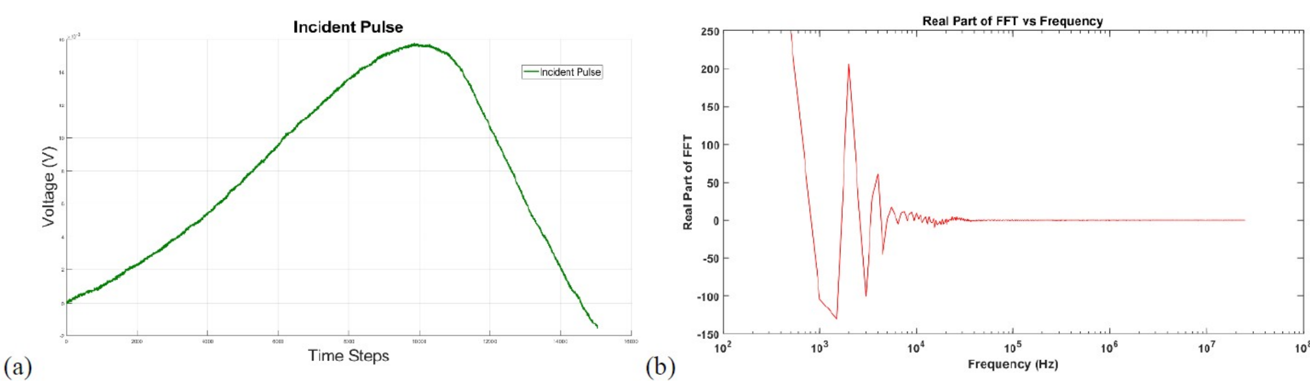

Fig. 6 (a) Incident load pulse (b) real part of FFT of incident signal to determine base frequency.

Measurements

The Kolsky bar setup consists of loading device which contains the gas gun, striker bar, incident bar, transmission bar, and momentum bar as shown in Figure 2. Strain gauges mounted on both bars measure the incident, reflected, and transmitted strain waves with the help of Wheatstone bridges and oscilloscope data [2]. To verify the viability of this setup, initial studies were performed on an Al 2024 specimen with a notch radius of 1.5mm. Figure 6 shows the overlay incident, reflected and transmitted signal.

The plot in Figure 8 determines the balance of stresses in incident and the transmitted bar. We can see a slight mismatch due to energy dissipation from the fixtures of four-point bend setup attached to the Kolsky Bar.

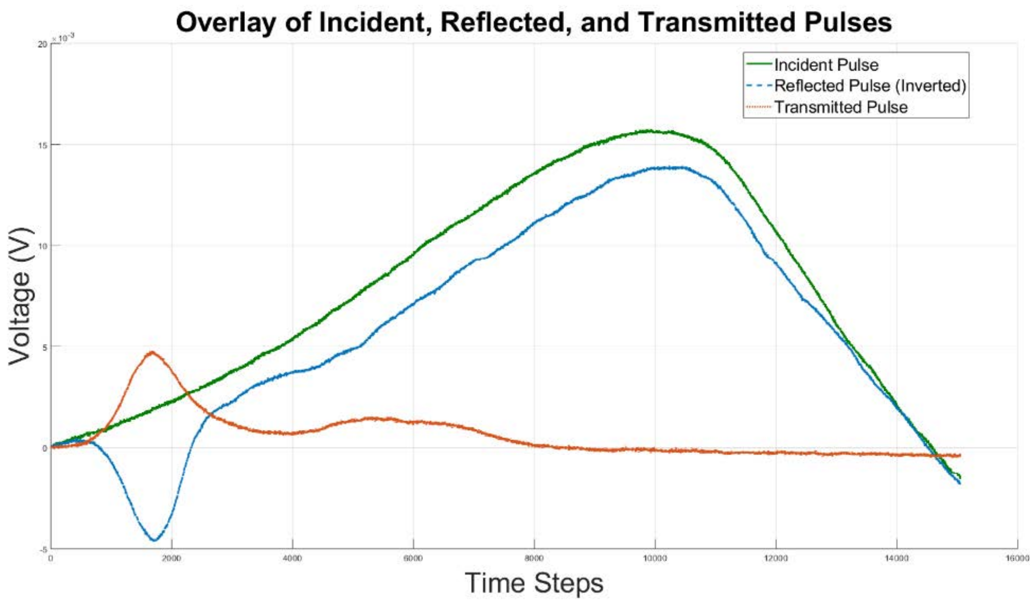

Fig. 7 The recorded incident, reflected and transmitted pulse data from the oscilloscope

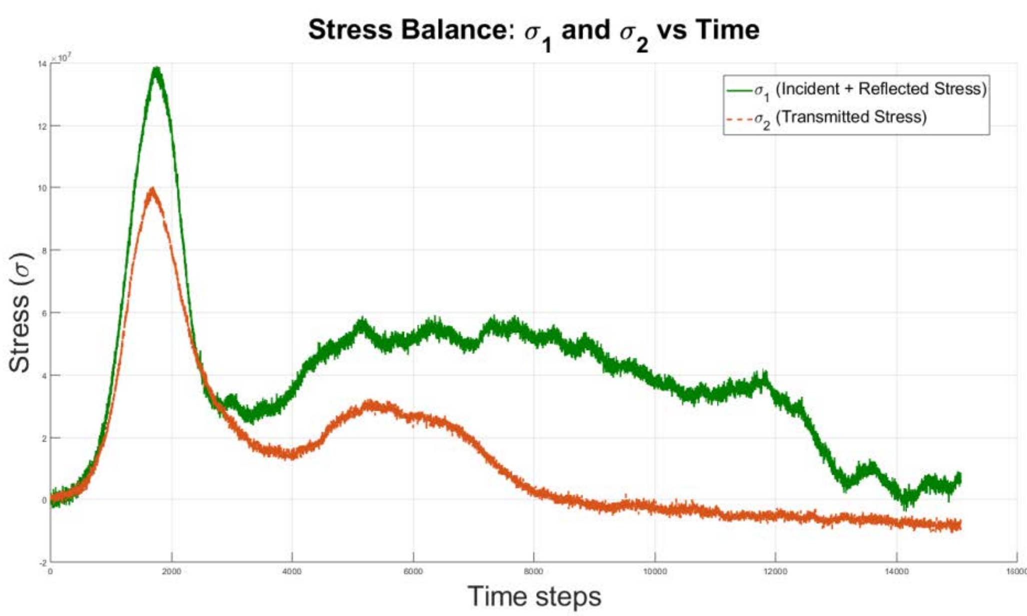

Fig. 8 Stress Balance to determine equilibrium

A high-speed camera is used to monitor the cracking of the specimen, the captured images are then used to perform DIC (Digital Image Correlation) to calculate local deformation. High speed images were captured using a Shimadzu HPV-X2 camera capable of up to 10 million frames per second (10 MHz framerate). The camera is orthogonally positioned to the bar axis. The HPV-X2 has a frame resolution of 400×250 pixels and records a maximum of 128 frames regardless of framerate.

A single Cordin Model 659 capacitive discharge flash lamp which was mounted beside the camera was used for consistent illumination. Delay timings are adjusted within the Shimadzu software to account for time taken by elastic wave propagated from strain gauge to the sample. Recorded camera frames are output from the HPV-X2 into the oscilloscope to correlate the captured image sequence frames to the corresponding load signals for post-impact analysis. The images from Shimadzu can be seen in Figure 9 at different loading conditions. The peak load calculated was 95483.21 N.

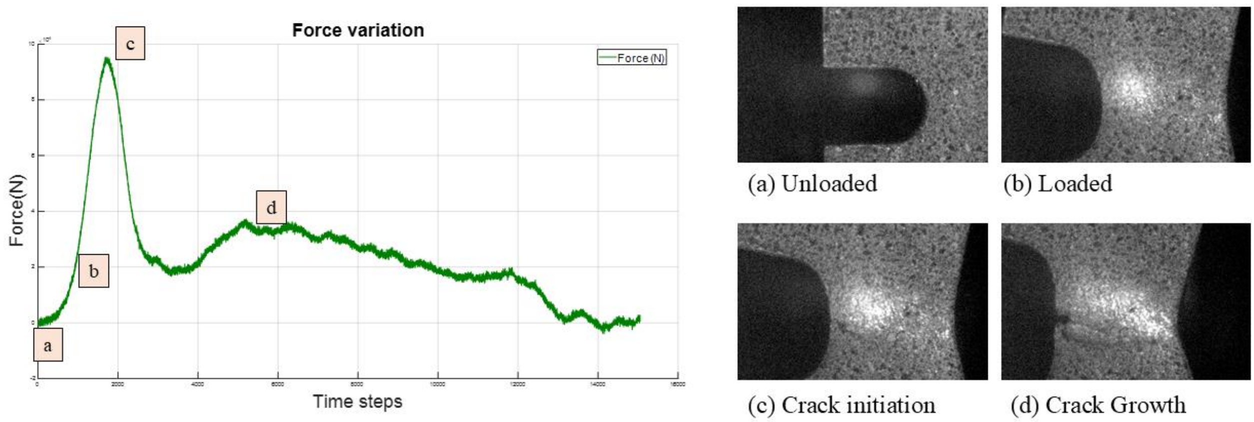

Fig. 9 Force and loading conditions

Triaxiality is an important parameter to determine material behavior under fracture. It is the ratio of hydrostatic stress to Von-Mises stress. The value determines the resistance for crack growth. Hence, higher stress triaxiality relates to brittle failure and cleavage and lower stress triaxiality values relate to micro-void coalescence and shear lip formation [14]. Quasi-static analysis was carried out for all geometries to evaluate the quasi-static variation of triaxiality factors at the notch tips respectively. The material model is taken as Johson-Cook Plasticity model with values from Leuser et al [5]. These values can be seen in the trend shown in Figure 10.

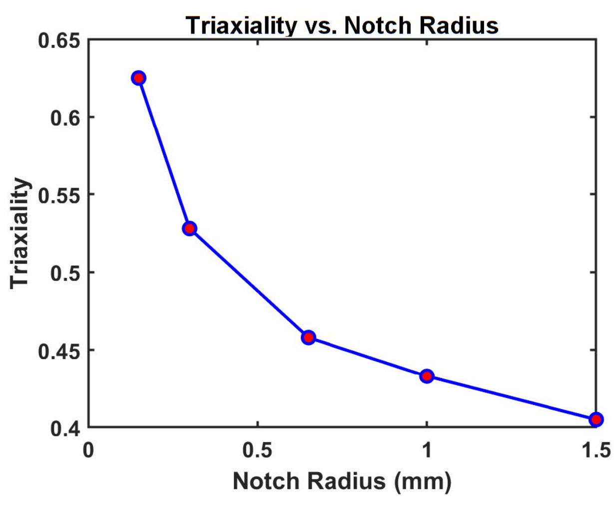

Fig. 10 Variation of stress triaxiality with notch radius from ABAQUS simulations.

Future Work

Specimens with the mentioned notch geometries for Al 2024 and Ti-6Al-4V will be conducted with the given experimental setup. The strain gauge data from the Kolsky Bar will be used to understand the loading conditions, calculate strain rate and the velocity of impact. DIC will be employed to evaluate and post process experimental data from high-speed camera to obtain fracture strain values. Simulations will be carried out in ABAQUS to obtain the stress triaxiality values. Correlation of fracture strain and triaxiality values will be done to establish a material model for elastic, plastic and crack initiation regimes for improved fracture predictions.

Conclusion

This study investigates Ti-6Al-4V and Al 2024 in a detailed experimental setup for the investigation of high-strain-rate fracture behavior using a modified SHPB setup with four-point bend fixtures. While the Johnson-Cook model has been used to simulate their deformation and failure, crack initiation at high triaxialities under high strain rates in Single Edge Notched Bend (SENB) specimens is conducted to establish a relationship between stress triaxiality and fracture strain at high strain rates. The notch sizes are varied to vary the stress triaxiality and the specimens are fractured in a single pulse of incident force to calculate fracture strain using DIC. To ensure dynamic equilibrium in the specimen, pulse shaping techniques are employed. As a part of future work, experiments will be conducted on Al 2024 and Ti-6Al-4V for different notch radii to identify fracture strain with the help of experiments and stress triaxiality with simulations and establish a relationship between them to create material models at high strain rates.

References

1. Weerasooriya, Tusit, Paul Moy, Daniel Casem, Ming Cheng, and Weinong Chen. “A four-point bend technique to determine dynamic fracture toughness of ceramics.” *Journal of the American Ceramic Society* 89, no. 3 (2006): 990-995.
2. Chen, Weinong W., and Bo Song. *Split Hopkinson (Kolsky) bar: design, testing and applications*. Springer Science & Business Media, 2010.
3. Williams, James C., and Rodney R. Boyer. “Opportunities and issues in the application of titanium alloys for aerospace components.” *Metals* 10, no. 6 (2020): 705.
4. Li, Shuang–Shuang, Xin Yue, Qing–Yuan Li, He–Li Peng, Bai–Xin Dong, Tian–Shu Liu, Hong–Yu Yang et al. “Development and applications of aluminum alloys for aerospace industry.” *Journal of Materials Research and Technology* (2023).
5. Lesuer, D. R. “Experimental investigations of material models for Ti-6Al-4V titanium and 2024-T3 aluminum. US Department of Transportation/Federal Aviation Administration.” *DTFA03–97Z-90007* (2000).
6. Wierzbicki, Tomasz, Yingbin Bao, Young-Woong Lee, and Yuanli Bai. “Calibration and evaluation of seven fracture models.” *International Journal of Mechanical Sciences* 47, no. 4-5 (2005): 719-743.
7. Wang, Bing, Xinran Xiao, Viktor P. Astakhov, and Zhanqiang Liu. “The effects of stress triaxiality and strain rate on the fracture strain of Ti6Al4V.” *Engineering Fracture Mechanics* 219 (2019): 106627.
8. Henschel, Sebastian, and Lutz Krüger. “Crack initiation at high loading rates applying the four-point bending split Hopkinson pressure bar technique.” *international Journal of Fracture* 201 (2016): 235-248.
9. ASTM International Committee E08 on Fatigue and Fracture. Subcommittee E08. 07 on Fracture Mechanics. *Standard Test Method for Linear-elastic Plane-strain Fracture Toughness K [Ic] of Metallic Materials*. ASTM international, 2023.
10. ASTM Committee E28 on Mechanical Testing and Subcommittee E28.07 on Impact Testing. *Standard Test Methods for Notched Bar Impact Testing of Metallic Materials.* ASTM international, 2024.
11. ASTM Committee C28 on Advanced Ceramics and Subcommittee C28.01 on Mechanical Properties and Performance. *Standard Test Method for Flexural Strength of Advanced Ceramics at Ambient Temperature.* ASTM international, 2018.
12. ASTM Committee A01 on Steel, Stainless Steel and Related Alloys and Subcommittee A01.29 on Tool Steels. *Standard Speci?cation for Tool Steels Alloy.* ASTM international, 2008.
13. Fischer-Cripps, Anthony C. *Introduction to contact mechanics*. Vol. 101. New York: Springer, 2007.
14. Anderson, Ted L., and Ted L. Anderson. *Fracture mechanics: fundamentals and applications*. CRC press, 2005.
15. Emmerling, W., D. Altobelli, K. Carney, and M. Pereira. “Development of a new metal material model in LS-DYNA Part 1: FAA, NASA, and industry collaboration background [DOT/FAA/TC-13/25].” *Federal Aviation Administration* (2014).
16. Buyuk M. *Development of A tabulated thermo-viscoplastic material model with regularized failure for dynamic ductile failure prediction of structures under impact loading.* [Order No. 3597748]. The George Washington University; 2013. *DOT/FAA/TC-13/25 Part 2*
17. Seidt, Jeremy Daniel. “Plastic deformation and ductile fracture of 2024-T351 aluminum under various loading conditions.” PhD diss., The Ohio State University, 2010. *DOT/FAA/TC-13/25 Part 3*
18. Haight, S., L. Wang, and P. Du Bois. *Development of a titanium alloy Ti-6Al-4V material model used in LS-DYNA DOT*. FAA/TC-15/23, 2016.
19. Haight, Sean Harrison. “An anisotropic and asymmetric Material Model for Simulation of Metals under dynamic Loading.” PhD diss., George Mason University, 2016. *DOT/FAA/TC-TT16/44*
20. Hammer, Jeremiah Thomas. “Plastic deformation and ductile fracture of Ti-6Al-4V under various loading conditions.” Master’s thesis, The Ohio State University, 2012. *DOT/FAA/TC-TT14/2*
21. Lesuer, Donald R. “Experimental investigations of material models for Ti-6Al-4V titanium and 2024-T3 aluminum.” *DOT/FAA/R-00/25* (2000).